Multidisciplinary Optimization of a Radial Compressor for Microgas Turbine Applications

T. Verstraete
e-mail: verstraete@vki.ac.be

Z. Alsalihi
e-mail: alsalihi@vki.ac.be

R. A. Van den Braembussche
e-mail: vdb@vki.ac.be

von Karman Institute for Fluid Dynamics,
Waterloose Steenweg 72,
1640 Sint-Genesius-Rode, Belgium

A multidisciplinary optimization system and its application to the design of a small radial compressor impeller are presented. The method uses a genetic algorithm and artificial neural network to find a compromise between the conflicting demands of high efficiency and low centrifugal stresses in the blades. Concurrent analyses of the aero performance and stress predictions replace the traditional time consuming sequential design approach. The aerodynamic performance, predicted by a 3D Navier–Stokes solver, is maximized while limiting the mechanical stresses to a maximum value. The stresses are calculated by means of a finite element analysis, and controlled by modifying the blade camber, lean, and thickness at the hub. The results show that it is possible to obtain a significant reduction of the centrifugal stresses in the blades without penalizing the performance.
[DOI: 10.1115/1.3144162]

1 Introduction

Microgas turbines are characterized by high rotational speeds (up to 2×10^6 rpm), with rotor diameters as low as 4 mm [1,2]. Designing turbomachines of this size results in new problems that still need to be solved. The small dimensions prevent blade cooling, and the large temperature differences over small distances result in large heat transfers and nonadiabatic flows. The high metal temperatures and large temperature gradients are other challenging aspects of the microgas turbine design in terms of mechanical integrity.

The small size favors the use of single stage 3D radial compressors and turbines (Fig. 1). High tip speeds (over 500 m/s) are needed to achieve the required pressure ratio. The corresponding centrifugal forces, proportional to the metal density and square of the tip speed, are at the origin of high mechanical stresses in the disk and the blades. Special materials, conserving strength at high temperatures and with low mass density, only partially alleviate the problem. A careful design is needed to respect the stress limitations without penalizing on aeroperformance.

Traditional approaches start with an aerodynamic design, in which the designer tries to define a high performing geometry. This geometry is then submitted to a finite element stress analysis (FEA), to verify that the maximum allowable stress in the material has not been exceeded. If so, the geometry is returned to the aerodesigner with restrictions on the design space, hoping that the next design will satisfy the mechanical requirements. Several iterations between the aerodesign and mechanical analysis may be needed before a satisfactory compromise is found.

The present paper reports on the design of a radial microcompressor, by means of a new multidisciplinary design method. It is based on a concurrent approach that searches for a global optimum, by considering simultaneously the aeroperformance and stress levels in the geometries. It aims for improved performance while respecting the mechanical constraints and shortening the design time and effort. The method is illustrated by the optimization of a radial impeller, 20 mm in diameter.

Contributed by the International Gas Turbine Institute of ASME for publication in the JOURNAL OF TURBOMACHINERY. Manuscript received August 1, 2008; final manuscript received February 26, 2009; published online March 24, 2010. Review conducted by David Wisler. Paper presented at the ASME Turbo Expo 2007: Land, Sea and Air (GT2007), Montreal, Quebec, Canada, May 14–17, 2007.

2 Optimization Method

The method is an extension of the aerodynamic optimization tool for radial impellers, developed at the von Karman Institute [3–5]. The system (Fig. 2) makes use of a genetic algorithm (GA), an artificial neural network (ANN), a database, a Navier–Stokes solver (NS), and a FEA. The basic idea of this method is a two-level optimization. The first one uses a rapid but less accurate analysis method (ANN), to evaluate the large number of geometries generated by the GA. The optimum geometry, according to the ANN predictions, is then analyzed by the more accurate but computationally much more expensive Navier–Stokes and FEA stress calculations, to verify the accuracy of the ANN predictions. The outcome of such an optimization cycle is added to the database. It is expected that, after a new training on the extended database, the ANN will be more accurate as it is based on more information, and the outcome of the next GA optimization will be closer to the real one. The optimization cycle is repeated until the Navier–Stokes and FEA results confirm the accuracy of the ANN predictions.

The extensions made to the existing optimization algorithm are: the stress predictions by the ANN, the FEA stress analysis in parallel with the Navier–Stokes calculations, the extension of the objective function with mechanical targets, and the use of extra design parameters to allow stress reductions.

2.1 Geometry Definition. The 3D radial compressor is defined by the meridional contour at the hub and shroud, the camber line of the main and splitter blade, the thickness distribution normal to the camber line, and the number of blades.

The hub and shroud meridional contours are defined by third order Bézier curves, between the leading and the trailing edge (Fig. 3). The coordinates of the control points are geometrical parameters that can be changed by the optimization program. The possible variations of the individual Bézier control points are shown by arrows in Fig. 3. The control point at the hub trailing edge is fixed by the prescribed outlet diameter. Several control points have only one degree of freedom because they are linked to other parameters, in order to guarantee an axial inlet or radial outlet. The shroud leading edge diameter defines the variable impeller inlet height.

Third order Bézier curves define also the inlet bend. Their control points are automatically adjusted to obtain a smooth link between the given radial inlet and the impeller. Only six parameters are needed to define the meridional contour. Each of them has a limited range, in which it can vary.

 Copyright © 2010 by ASME

Downloaded 28 May 2010 to 128.113.26.88. Redistribution subject to ASME license or copyright; see http://www.asme.org/terms/Terms_Use.cfm

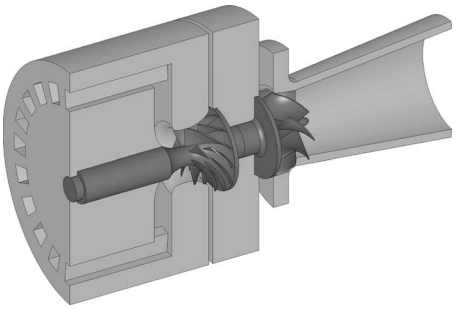

Fig. 1 Layout of a microgas turbine; schematic view on the electrical generator, compressor and turbine

The blade camber lines at the hub and shroud are defined by the distribution of the angle $\beta(u)$, between the meridional plane m and the blade camber (Fig. 4). The β distributions at the hub and shroud are defined by third order polynomials (Eq. (1)), with u the nondimensional meridional length ($u \in [0,1]$, 0 at the leading edge and 1 at the trailing edge). The camber line circumferential position θ (Fig. 4) is then defined by Eq. (2)

$$\beta(u) = \beta_0(1-u)^3 + 3\beta_1 u(1-u)^2 + 3\beta_2 u^2(1-u) + \beta_3 u^3 \quad (1)$$

$$Rd\theta = dm \tan \beta \quad (2)$$

β_0 and β_3 are the blade angles at leading and trailing edge. This definition is used for both the main and splitter blade, at the hub and shroud. The splitter trailing edge blade angles are the same as the full blade values at the hub and shroud. This results in 14 design variables for the blade camber line definition.

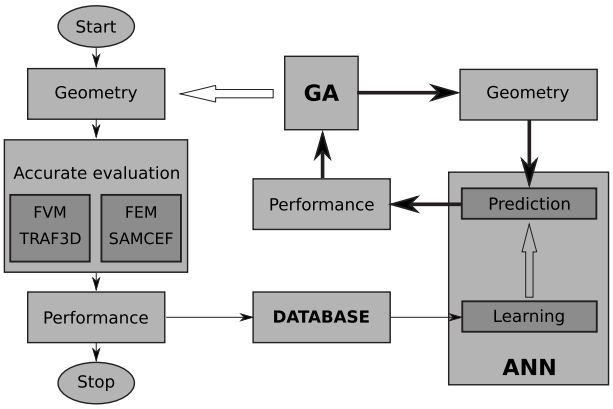

Fig. 2 Flow chart of the optimization algorithm

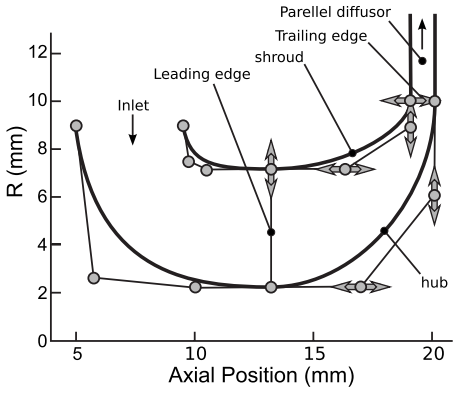

Fig. 3 Meridional contour defined by Bézier control points

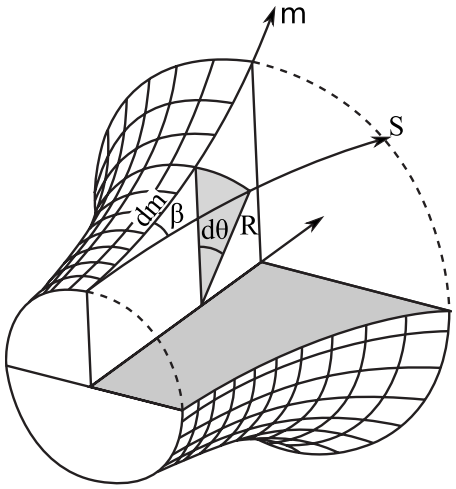

Fig. 4 Definition of the blade camber line by β angle

The streamwise position of the splitter blade leading edge is also a design parameter. It is defined as a percentage of the main blade camber length and can vary between 20% and 35%.

The blade thickness distributions at the hub and shroud are the function of two parameters: the thickness *LE* of the ellipse defining the leading edge, and the trailing edge thickness *TE* (Fig. 5). The blade thickness is fixed at the shroud ($LE=TE=0.3$ mm). The two parameters defining the blade thickness at the hub are design parameters, and can vary between 0.3 mm and 0.6 mm. The same values are used for the main and splitter blades.

The number of blades could also be a design parameter to be optimized, but has been fixed to seven for manufacturing reasons. This brings the total number of design parameters to 23.

2.2 NS Solver. The TRAF3D Navier–Stokes solver [6] is used to predict the aerodynamic performance of the radial compressors. Structured H-grids with $2\times216\times48\times52$ (1,080,000 cells) are used for all computations to guarantee a comparable accuracy for all the samples stored in the database. All computations are nonadiabatic with the specified wall temperature to account for the heat transfer from turbine to compressor.

2.3 FEA . The commercial code SAMCEF [7] is used for the stress calculation. Quadratic tetrahedral elements are used as a compromise between element quality and automatic meshing. Similar grids with 250,000 nodes and 160,000 elements are used for all samples. The grid is refined in areas of stress concentrations. Periodic boundary conditions are applied, such that only a one-seventh part of the geometry needs to be analyzed.

2.4 The ANN. The ANN used in present study is the "SNNS," developed at the institute for Parallel and Distributed High Performance Systems of the University of Stuttgart [8]. Eight individual ANNs are used: one, to predict the efficiency, two, to predict the mass flow in the channels on both sides of the

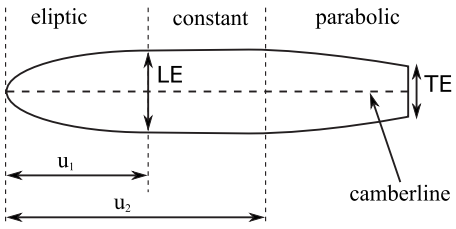

Fig. 5 Thickness distribution along the camber line of the blade (not to scale)

Downloaded 28 May 2010 to 128.113.26.88. Redistribution subject to ASME license or copyright; see http://www.asme.org/terms/Terms_Use.cfm

splitter, four ANNs predict the Mach number distribution, respectively, at the hub and shroud of the full blades and splitter blades, and one predicts the maximum stress in the geometry. This split into dedicated ANNs, enhances the accuracy by which important values such as efficiency and maximum stress can be predicted.

2.5 The GA. The GA used in the present work is the one developed by Carroll and co-workers [9] at the University of Illinois. Typically, 100 generations are created, each containing 50 individuals. The parameters of the GA have been optimized in a previous study [10].

2.6 The Database. The accuracy of the ANN predictions strongly depends on the information contained in the database. The design of experiments (DOE) method is used to create the initial database. This maximizes the amount of information contained in it, for a limited number of geometries [11].

Each design variable can take two values, fixed at 25% and 75% of the maximum design range. A 2^{k-p} factorial design is used. k is the total number of design parameters (23), while p defines the number of lower order parameter combinations that are not analyzed. p is fixed at 17, which results in a total of $2^6=64$ samples in the initial database.

3 The Performance

The compressor optimization is driven by an objective function (OF), that increases with decreasing aeroperformance, and when the aero and mechanical requirements are not met. It is the weighted sum of several penalties, given by Eq. (3)

$$OF(\boldsymbol{G}) = w_{\text{stress}} \cdot P_{\text{stress}}(\boldsymbol{G}) + w_{\eta} \cdot P_{\eta}(\boldsymbol{G}) + w_{\text{massflow}} \cdot P_{\text{massflow}}(\boldsymbol{G}) + w_{\text{Mach}} \cdot P_{\text{Mach}}(\boldsymbol{G}) \tag{3}$$

The first penalty (Eq. (4)) concerns the mechanical stresses, where $\sigma_{\max}$ is the maximum stress in the impeller. This penalty is zero when the stresses are below the allowable limit $\sigma_{\text{allowable}}$ and increases linearly when the von Mises stresses exceed that value. This weak formulation of the constraint does not guarantee that it is fully respected. However, it has the advantage that all geometries, that have been analyzed, lead toward the optimum geometry

$$P_{\text{stress}} = \max\left[\frac{\sigma_{\max} - \sigma_{\text{allowable}}}{\sigma_{\text{allowable}}}, 0.0\right] \tag{4}$$

The second term in the objective function is the efficiency penalty (Eq. (5)), and it decreases with increasing total to static polytropic efficiency. The required efficiency η_{req} is usually set to an unachievable values (for instance 1.0), so that, unlike the other penalties, its value never goes to zero. It means that the efficiency can still be maximized, once all other requirements are met

$$P_{\eta} = \max(\eta_{\text{req}} - \eta, 0.0) \tag{5}$$

The third penalty concerns the mass flow and it has two contributions: a penalty on incorrect mass flow (Eq. (6)), and a penalty on the difference in mass flow (Eq. (7)). The first one increases when the mass flow differs from the required one, by more than 0.33%.

The second one penalizes the difference in mass flow on both sides of the splitter blade

$$P_{\text{mass flow}} = \left(\max\left[\left(\frac{|\dot{m}_{\text{req}} - \dot{m}|}{\dot{m}_{\text{req}}} - \frac{1}{300}\right), 0.0\right]\right)^2 \tag{6}$$

$$P_{\text{mass diff}} = \left(\frac{\dot{m}_{\text{upper}} - \dot{m}_{\text{lower}}}{\dot{m}_{\text{upper}} + \dot{m}_{\text{lower}}}\right)^2 \tag{7}$$

The penalty on the Mach number aims to favor Mach number distributions that are expected to remain also good at off-design operations. It has two contributions. The first one (Eq. (8)) penalizes negative loading, and is proportional to the area between the suction and pressure side, when the pressure side Mach number is higher than the suction side (Fig. 6). Areas of negative loading result in extra friction losses, without contribution to the pressure rise.

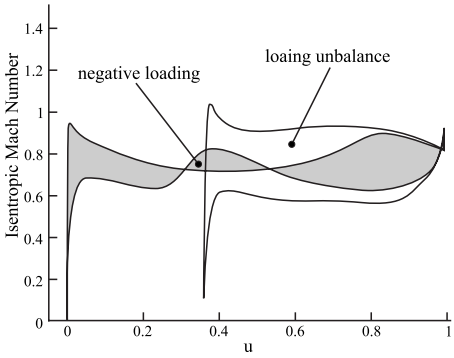

Fig. 6 Negative loading and loading unbalance in a compressor with splitter vanes

The second Mach penalty (Eq. (9)) increases with the loading unbalance between main blade and splitter blade. This penalty compares the area between the suction and pressure side Mach number distribution of main blade A_{bl} and splitter blade A_{sp}, corrected for the difference in blade length (Fig. 6).

$$P_{\text{Mach}} = \int_0^1 \max[M_{\text{ps}}(s) - M_{\text{ss}}(s), 0.0] \cdot ds \tag{8}$$

$$P_{\text{loading unbalance}} = \left(\frac{A_{\text{bl}} - A_{\text{sp}}}{A_{\text{bl}} + A_{\text{sp}}}\right)^2 \tag{9}$$

The weights in the objective function depend on the application, and allow emphasizing on performance or on mechanical integrity.

4 Design Conditions

The method has been used to optimize a radial compressor with a diameter of 20 mm, rotating at 500,000 rpm. The corresponding tip speed of 523.6 m/s, results in very high centrifugal stresses. Titanium TI-6AL-4V has been selected for its high yield stress over mass density ratio ($\sigma_{\text{yield}}/\rho$). The characteristics used in the calculation are as follows: elasticity modulus$=113.8\times10^{+9}$ Pa, Poisson modulus$=0.342$, and mass density$=4.42\times10^{+3}$ kg/m^3.

The computational domain starts at constant radius in the radial inlet (Fig. 3) and ends in the vaneless diffuser at $r/r_2=1.5$ (Fig. 1). Part of the hub surface at the inlet (for $r<4$ mm) rotates because it connects the compressor shaft to the electric generator.

The disk thickness at the compressor rim is 1 mm. It is connected to an 8 mm diameter shaft, with a fillet of 2 mm radius (Fig. 1), all made of one piece. A fillet radius of 0.25 mm is applied at the blade hub to limit the local stress concentrations.

The unshrouded impeller has a tip clearance of 0.1 mm, which is 10% of the exit blade height and is typical for these small impellers. It is one of the reasons for the moderate efficiencies.

The weight factors of the objective function are determined, based on the knowledge gained in previous optimizations. The constants and weights, defining the penalties in the present design, are listed in Table 1. Taking into account the difference in weight factors, an efficiency drop of 1% is as penalizing as an excess in stress limit of $40/24=1.667\%$ (or 6.668 MPa).

The total inlet temperature is 293 K and the total inlet pressure is $1.013\times10^{+5}$ Pa. The design mass flow is 20 g/s at a pressure ratio of 3 (total to static). The wall temperature of the impeller is fixed at 400 K, as found in a previous study on the heat transfer inside the entire microgas turbine [12]. The maximum allowable stress is a function of the material temperature. A large safety

Downloaded 28 May 2010 to 128.113.26.88. Redistribution subject to ASME license or copyright; see http://www.asme.org/terms/Terms_Use.cfm

Table 1 List of penalty parameters and weight factors

Allowable stress	400 MPa
Stress penalty weight	24.0
Efficiency required	0.825
Efficiency penalty weight	40.0
Mass flow required	20.0 g/s
Mass flow penalty weight	18.0
Mass flow difference weight	20.0
Mach negative loading weight hub	15.0
Mach negative loading weight shroud	24.0
Mach loading unbalance weight hub	1.0
Mach loading unbalance weight shroud	1.5

margin is used to account for vibrations and possible local temperature peaks, resulting in a maximum allowable value of 400 MPa.

The multidisciplinary optimization starts from the result of a simple aerodynamic optimization without stress analysis. It is called the "baseline" impeller. Although this geometry has a good efficiency, it cannot be used because a mechanical stress analysis predicts von Mises stresses in excess of 750 MPa. It serves as a reference for further optimizations.

An initial database containing a total of 53 geometries is used at the start. 13 geometries out of the 64, defined by the DOE technique, could not be analyzed because of geometrical constraints (intersection of the main blade with the splitter blade). Two additional geometries have been added, namely, the baseline geometry and the central case. The latter one is a geometry with all parameters at 50% of their range.

5 Results

Figure 7 shows the convergence history of the optimization. The "aeropenalty," based only on Navier–Stokes predictions of efficiency, Mach number distribution and mass flow, the "stress penalty" based on the result of the FEA analyses, and "total penalty" are compared with the ones predicted by the ANN. One observes a decrease in the discrepancy, between both prediction methods with iteration number. This is the consequence of an increasing number of samples in the database, resulting in a more accurate ANN.

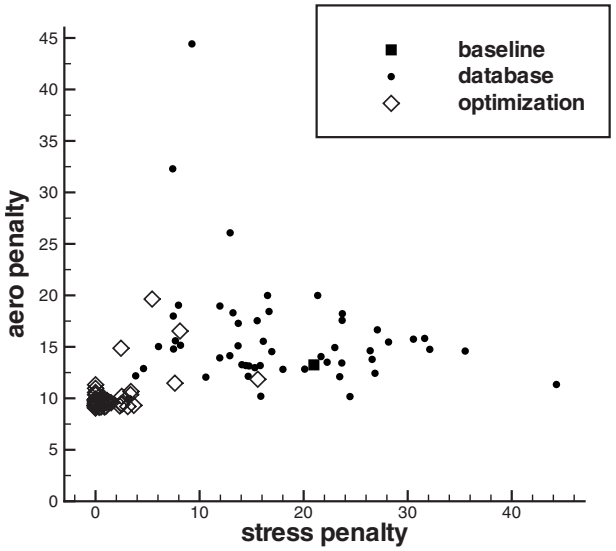

Fig. 8 Aero penalty versus stress penalty for baseline, database, and optimization geometries

Only ten iterations are needed to obtain a very good agreement for the aeropenalty. The ANN stress penalty is zero, for every geometry proposed by the GA. However, it takes more than 15 iterations, before the FEA confirms that the proposed geometries satisfy the mechanical requirements.

The good agreement in both stress- and aeropenalties, over the last 18 iterations, indicates that the ANN predictions are reliable. It means that the same optimum geometry would have been obtained if the GA optimization had been based on the more sophisticated NS and FEA analyses. Hence, no further improvement can be expected. The optimization procedure could have already been stopped after 35 iterations.

The aeropenalty is plotted versus the stress penalty in Fig. 8. The geometries created during the optimization process are all in the region of low penalties. Most of them outperform the geometries of the database. Only a few geometries have penalties of the

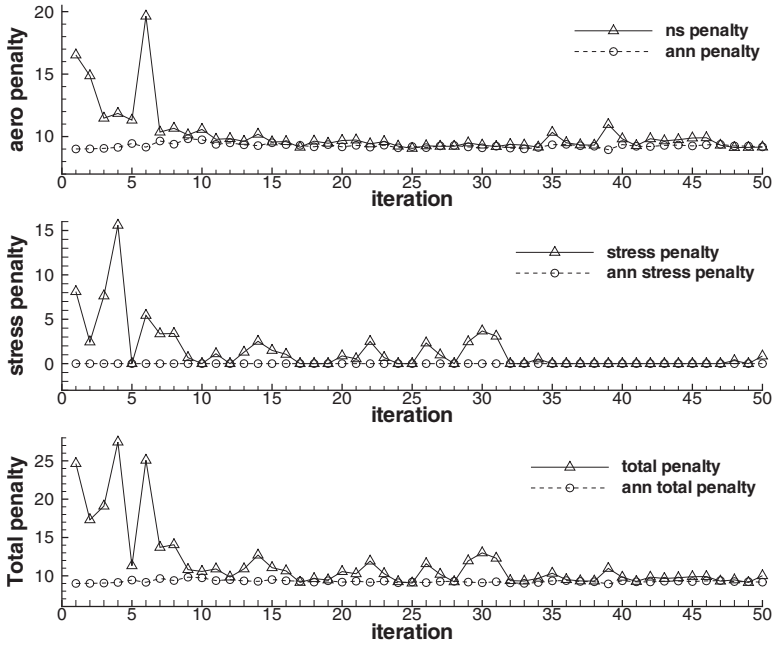

Fig. 7 Convergence history of the optimization

Downloaded 28 May 2010 to 128.113.26.88. Redistribution subject to ASME license or copyright; see http://www.asme.org/terms/Terms_Use.cfm

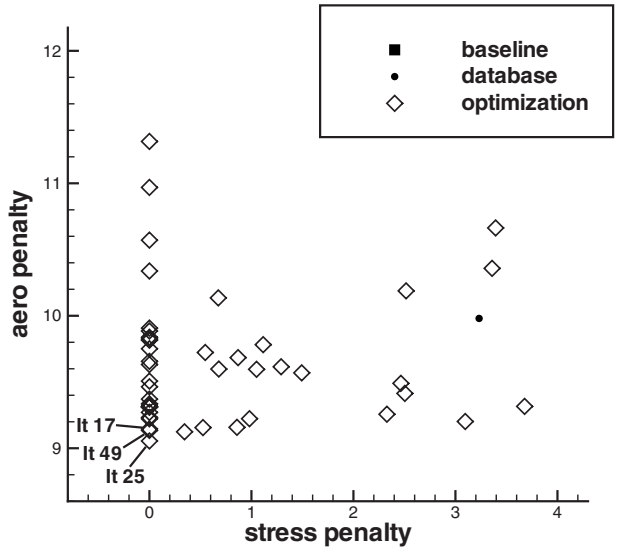

Fig. 9 Zoom on the low penalty region of Fig. 8

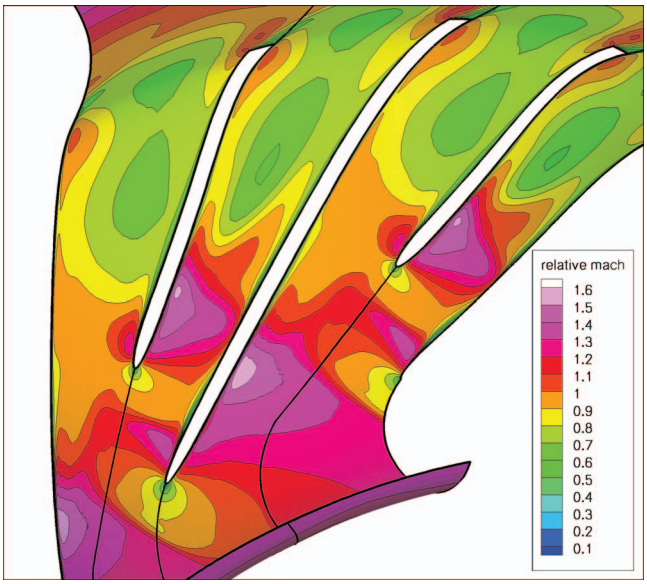

Fig. 10 Isentropic Mach number plot at 90% of the span (near the tip) of geometry 25

same order as the database samples. Those geometries are the ones created during the first ten iterations, where the ANN is still inaccurate.

Figure 9 is a zoom on the low penalty region of Fig. 8. A large number of geometries have zero stress penalties but with different aeropenalty. The geometries corresponding to iteration 17, 49, and 25 have the lowest aeropenalty. Iteration 2 has the highest efficiency (60.4%), but has a high aeropenalty due to negative loading and loading unbalance. Results of iteration 2, 17, 25, and 49 are compared with the baseline in Table 2.

In spite of its high efficiency, the baseline impeller shows a high aeropenalty because of a too high mass flow. Among all the geometries created during the optimization, iteration 25 performed the best. It has a little lower efficiency than iteration 17, but less loading unbalance, and the stresses are 33 MPa below the limit. The influence of the stress penalty on the optimization is clear by comparing the values of the baseline impeller with the ones of iteration 25. The reduction of the maximum stress level with 370 MPa is at the cost of a 2.3% decrease in efficiency.

The iso-Mach number plot, at 90% span (near the tip) of iteration 25, is shown in Fig. 10. Near choking flow appears at the leading edge of the main blade. This is the consequence of the radial to axial turn of the inlet duct, resulting in an increased absolute velocity at the tip section.

Figures 11 and 12 compare the von Mises stresses in the baseline geometry with the ones of iteration 25. The drastic reduction in stress is due to the following:

- the reduced blade height at the leading edge, resulting in lower centrifugal forces at the leading edge hub
- the increase in blade thickness at the hub
- the modified blade curvature resulting in less bending by centrifugal forces

The blade lean is defined as the angle between the leading edge and the meridional plane (positive in the direction of rotation). It is a result of the integration of the β distribution at the hub and shroud, when the trailing edge rake is limited to 45 deg. Lean can be as low as −15.0 deg (see Table 2, iteration 49), without exceeding the maximum stress limit.

Figure 13 shows the impact of the leading edge lean on stress and efficiency. One observes a rather clear relation between lean and stress. The lowest stresses are observed around −15.0 deg. Several geometries with good efficiency are found for lean angles between −40.0 deg and −5.0 deg. The drop in efficiency for lean angles above −5.0 deg suggests that in the present application, the best impellers have some negative lean.

Figure 14 shows the stress and efficiency, versus blade thickness at the leading edge for all geometries. The nondimensional values 0 and 1 correspond to a blade thickness of 0.3 mm and 0.6 mm, respectively. The database geometries are the ones at 25% or 75% of the range, together with the central case and the baseline. Although a lot of stress variation is still possible at each thickness, the lowest stress level for the database samples at 25% (0.375 mm blade thickness) is noticeable, higher than at 75% (0.575 mm blade thickness). It shows that blades with thicker hub sections are more likely to have a lower maximum stress than thin ones. However, an appropriate choice of the other parameters is still needed to reduce the stresses below the 400 MPa limit. A good blade

Table 2 Comparison of optimized geometries with the baseline geometry

	Baseline	It 2	It 17	It 25	It 49
t-s efficiency	62.34	60.42	60.31	60.06	59.68
Aeropenalty	13.24	14.86	9.14	9.05	9.14
Loading unbalance penalty	0.06	3.84	0.26	0.04	0.00
Max von Mises (MPa)	749	440	389	367	396
Blade lean	−7.8 deg	−11.8 deg	−8.6 deg	−7.3 deg	−15.0 deg
Mass flow (g/s)	25.9	19.6	20.2	20.2	20.1
Power (kW)	3.19	2.52	2.61	2.62	2.62
Specific power (W s/kg)	123.2	128.6	129.2	129.7	130.3

Downloaded 28 May 2010 to 128.113.26.88. Redistribution subject to ASME license or copyright; see http://www.asme.org/terms/Terms_Use.cfm

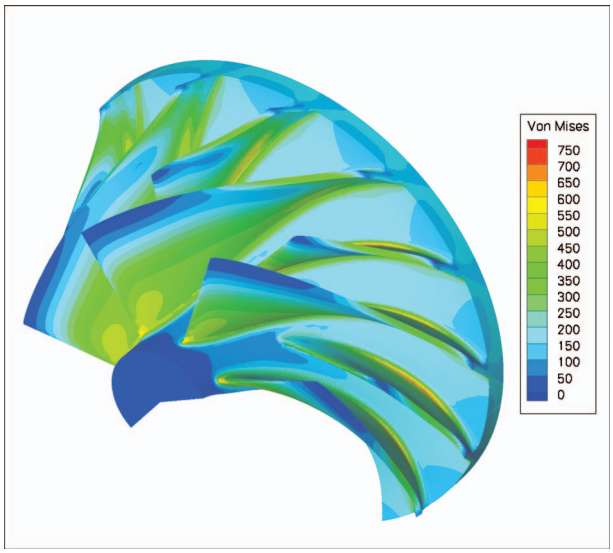

Fig. 11 von Mises stresses due to centrifugal loading in the baseline

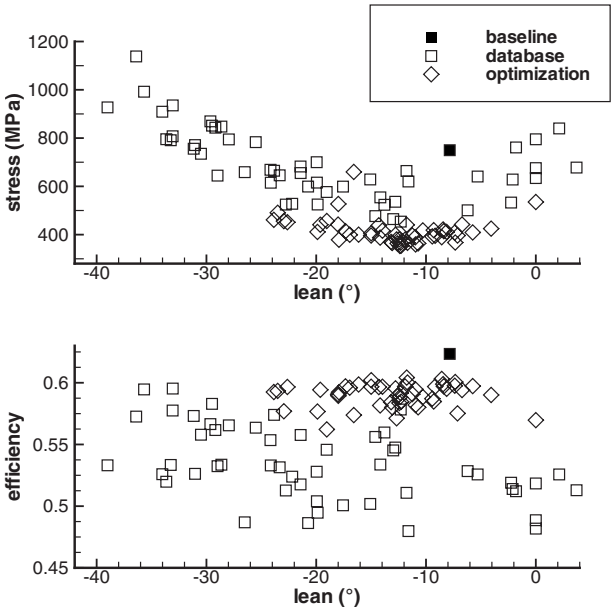

Fig. 13 Blade lean versus stress and efficiency for database and optimization geometries

thickness is not necessarily at its maximal value. The LE thickness (see Fig. 5) of geometry 25 is 0.58 mm, which is at 93% of the range.

The average efficiency of the database samples at 25% is comparable to the ones at 75% thickness, suggesting that the hub leading edge thickness does not have much impact on efficiency. Hence, the high efficiencies of the geometries, created during the optimization process, are due to an optimum choice of the other design parameters. Also the trailing edge thickness (Fig. 5) has a negligible influence on stress and efficiency.

Figure 15 shows the impact of the leading edge blade height on the stress and efficiency. The radius at the LE shroud (see Fig. 3) can vary between 6.5 mm and 7.5 mm, resulting in a blade height of 4.25 mm and 5.25 mm, respectively.

Shortening the blades lowers the stresses, but the database samples show a small drop in efficiency. This explains the difficulty to maintain high efficiency when reducing the stress. However, the optimized geometries have shorter vanes, and show a high efficiency. This indicates that the efficiency also depends on an optimum choice of other parameters.

Figure 16 shows a large impact of the trailing edge blade height on efficiency. The trend is very clear, and all geometries created during the optimization are near the minimum blade height. It suggests that a smaller blade height could even be better. However, the minimum blade height is limited by manufacturing constraints. The blade height has a small impact on the maximum stress in the impeller.

The other design parameters have a less pronounced influence on stress and efficiency. The latter depends more on a combination of several parameters than on individual parameter changes. This illustrates the strongly coupled nature of the design problem, and the need for an optimization tool.

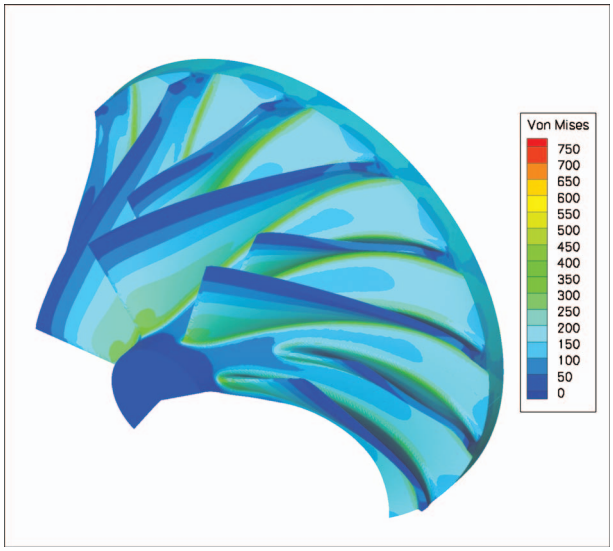

Fig. 12 von Mises stresses due to centrifugal loading in iteration 25

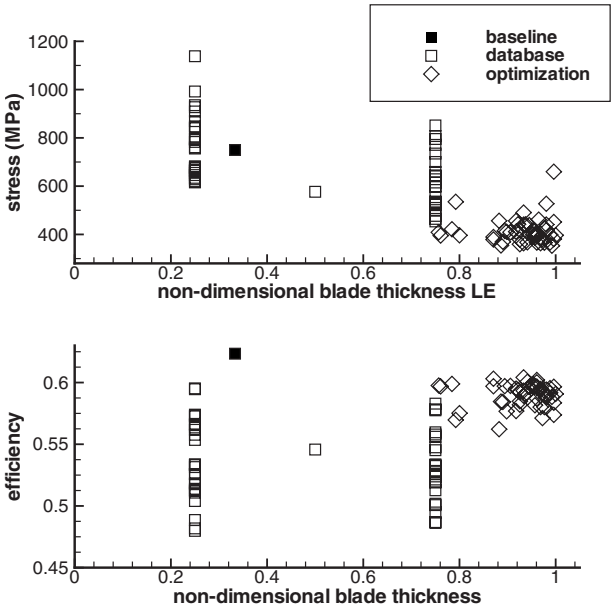

Fig. 14 Stress and efficiency versus blade hub leading edge thickness for database and optimization geometries

Downloaded 28 May 2010 to 128.113.26.88. Redistribution subject to ASME license or copyright; see http://www.asme.org/terms/Terms_Use.cfm

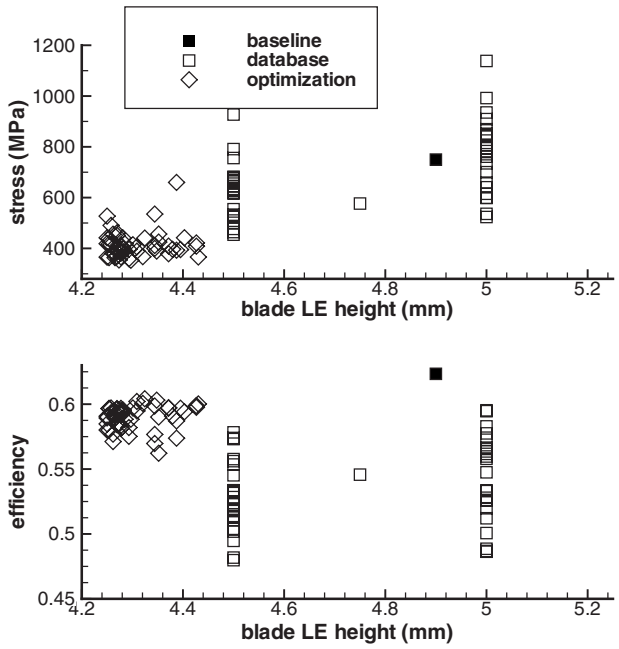

Fig. 15 Blade leading edge height versus stress and efficiency

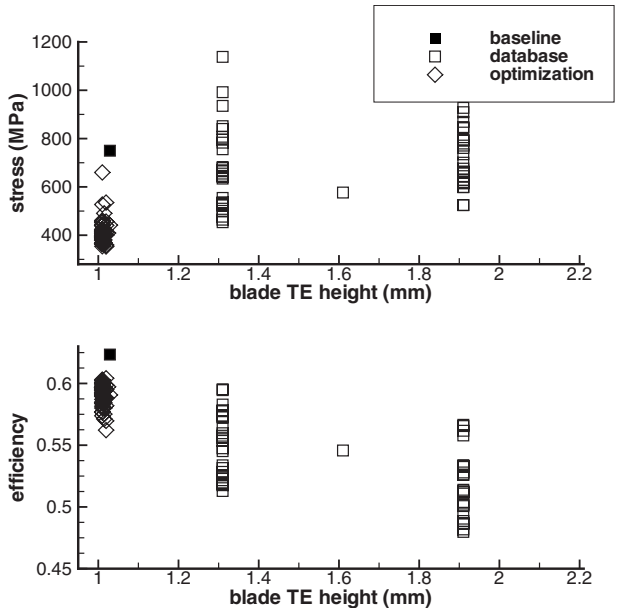

Fig. 16 Blade trailing edge height versus stress and efficiency for database and optimization geometries

6 Conclusions

A fully automatic concurrent optimization system is developed and successfully used for the multidisciplinary optimization of a radial compressor for a micro gas turbine application. It is shown that the stresses can be drastically reduced, with only a small decrease in efficiency.

The main parameters that allow a reduction of the stresses have been identified. They are the following.

- The blade thickness at the hub. Increasing it contributes to a decrease in von Mises stresses with a negligible impact on aeroperformance.
- The blade leading edge lean and height. They have a direct impact on the von Mises stresses. The impact on performance can be compensated by other parameters.
- The trailing edge blade height. It has a direct influence on the aeroperformance but only a small impact on stresses.
- The blade curvature. It significantly influences both the aero and mechanical performance. However, it depends on a large number of parameters and the optimization algorithm is needed to find the optimum combination.

Acknowledgment

This research is sponsored by the Institute for the Promotion of Innovation by Science and Technology (IWT) in Flanders, Belgium, Project No. SBO 030288 "PowerMEMS."

Nomenclature

A = area
$\boldsymbol{G}$ = geometry vector
m = meridional length
$\dot{m}$ = mass flow
M = Mach number
P = penalty
r = radius
u = nondimensional meridional length
w = weight factor
β = blade angle from meridional (deg)
η = total to static polytrophic efficiency
θ = circumferential position (rad)
σ = mechanical stress

Subscripts

max = maximum value
allowable = allowable value
req = required value
ps = pressure side
ss = suction side
sp = splitter blade
bl = main blade

References

[1] Isomura, K., Murayama, M., and Kawakubo, T., 2001, "Feasibility Study of a Gas Turbine at Micro Scale," ASME Paper No. GT2001–GT-101.
[2] Epstein, A. H., 2004, "Millimeter-Scale, Micro-Electro Mechanical System Gas Turbine Engines," ASME J. Eng. Gas Turbines Power, **126**, pp. 205–226.
[3] Pierret, S., and Van den Braembussche, R. A., 1999, "Turbomachinery Blade Design Using a Navier Stokes Solver and Artificial Neural Networks," ASME J. Turbomach., **121**, pp. 326–332.
[4] Cosentino, R., Alsalihi, Z., and Van den Braembussche, R. A., 2001, "Expert System for Radial Impeller Optimization," *Proceedings of the Fourth European Conference on Turbomachinery*, Firenze, Italy, pp. 481–490.
[5] Rini, P., Alsalihi, Z., and Van den Braembussche, R. A., 2001, "Evaluation of a Design Method for Radial Impellers Based on Artificial Neural Network and Genetic Algorithm," *Proceedings of the Fifth ISAIF Conference*, Gdansk, Poland, pp. 535–543.
[6] Arnone, A., 1994, "Viscous Analysis of Three-Dimensional Rotor Flow Using a Multigrid Method," ASME J. Turbomach., **116**, pp. 435–445.
[7] SAMCEF FEA code by Samtech Group, www.samcef.com.
[8] Zell, A., Korb, Th., Sommer, T., and Bayer, R., 1990, "Applications of Neural Networks," *Conference Proceedings SPIE's Aerospace Sensing International Symposium*, Vol. 1294, pp. 16–20.
[9] Yang, G., Reinstein, L. E., Pai, S., Xu, Z., and Carroll, D. L., 1998, "A New Genetic Algorithm Technique in Optimization of Permanent ^{125}I Prostate Implants," Med. Phys., **25**, pp. 2308–2315.
[10] Harinck, J., Alsalihi, Z., Van Buijtenen, J. P., and Van den Braembussche, R. A., 2005, "Optimization of a 3D Radial Turbine by Means of an Improved Genetic Algorithm," *Proceedings of the Fifth European Conference on Turbomachinery*, Lille, France, pp. 1033–1042.
[11] Montgomery, D., 2001, *Design and Analysis of Experiments*, Wiley, New York.
[12] Verstraete, T., Alsalihi, Z., and Van den Braembussche, R. A., 2007, "Numerical Study of Heat Transfer in Micro Gas Turbines," ASME J. Turbomach., **129**(4), pp. 835–841.

Downloaded 28 May 2010 to 128.113.26.88. Redistribution subject to ASME license or copyright; see http://www.asme.org/terms/Terms_Use.cfm